EVALUATING THE IMPACT TRIGGER HYPOTHESIS FOR THE ONSET OF THE PALEOCENE-EOCENE THERMAL MAXIMUM

By

RYAN ALEXANDER GALINKIN

A thesis submitted to the

School of Graduate Studies

Rutgers, The State University of New Jersey

In partial fulfillment of the requirements

For the degree of

Master of Science

Graduate Program in Physics and Astronomy

Written under the direction of

Sonia Tikoo-Schantz

And approved by

_____

_____

_____

_____

New Brunswick, New Jersey

May, 2019

ABSTRACT OF THE THESIS

Evaluating the Impact Trigger Hypothesis for the Onset of the Paleocene-Eocene Thermal Maximum

by RYAN ALEXANDER GALINKIN

Thesis Director:

Sonia Tikoo-Schantz

We investigate whether an extraterrestrial impact could produce changes in atmospheric chemistry sufficient to produce the 5°C global temperature rise observed at the onset of the Paleocene-Eocene Thermal Maximum (PETM), a major global warming event in Earth history that occurred approximately 55.8 million years ago (Ma) [Charles et al., 2014]. We calculated greenhouse gas production stemming from both asteroidal and cometary impacts for impactors with radii of 2.5 km or 5 km, and impact angles perpendicular to the surface. We examined a range of processes such as fireball-induced combustion and associated release of biogenic carbon, the deposition of carbon and water directly from the impactor, the massive vaporization of water due to a deep oceanic impact, and the production of NO via a hypervelocity impactor's path through the atmosphere and subsequent O_3 production. We then convert the global warming potential (GWP) of the greenhouse gases produced in our calculations into GWP equivalent of CO_2 and use the resulting values to compute the estimated global increase in temperature for each hypothetical impact. Our most powerful impacts could potentially increase the global temperature by up to 4.69°C. This amount of warming is very close to what is inferred from paleoclimate records. We suggest that a purely perpendicular impact in our modeled size range is unlikely, yet plausible, to produce the required GWP equivalent of CO_2 to result in

a 5°C rise in global temperatures. However, future work may be conducted to study whether changes in impact angle may produce higher amounts of greenhouse gases and potentially be responsible for the abrupt warming experienced at the PETM boundary.

ACKNOWLEDGEMENTS

I would first like to thank my thesis advisor Dr. Tikoo of the department of Earth and Planetary Sciences at Rutgers, The State University of New Jersey for her patience, motivation, and knowledge. Her guidance helped me throughout my research and writing of this thesis. I could not have imagined having a better advisor and mentor.

I would like to express my sincere gratitude to Dr. Aubry, also of the department of Earth and Planetary Sciences at Rutgers University. She was instrumental in introducing me to Professor Tikoo, and she fostered my love of the planetary sciences. For six years she continued to support me in my endeavors, through both the good and the bad, and for that I cannot thank you enough.

I thank my fellow classmates for the stimulating discussions, for the sleepless nights working together before deadlines, and for all the fun we have had during the last two years. Without such an active support system this couldn't have been possible.

Finally I would like to thank my Mother and Father for their unwavering encouragement throughout my years of study; I couldn't have succeeded without your continuous support and guidance.

Table of Contents

List of Tables

List of Illustrations

1. Introduction

At the end of the Paleocene epoch, Earth experienced a short (∼20,000 years) but intense episode of global warming, which serves as a natural laboratory for understanding and predicting changes associated with current global warming. This event, known as the Paleocene-Eocene Thermal Maximum (PETM), occurred roughly 55.8 million years ago (Ma) and produced a 4-5°C rise in the temperature of the deep ocean [McInerney & Wing, 2011; Zachos et al., 2005] and equatorial regions [Bowen et al., 2014; Dickens, Castillo & Walker, 1997] of the planet, and an even larger, 6-8°C, rise in temperature towards the poles [Dickens et al., 1997; Retallack et al., 1997]. This warming is implied by a sudden decrease in the ratio of $^{18}O/^{16}O$ (known as an oxygen isotope excursion) preserved in ancient benthic and planktonic foraminifera shells recovered from deep sea cores (See Figure 1) [Kennet & Stott, 1991].

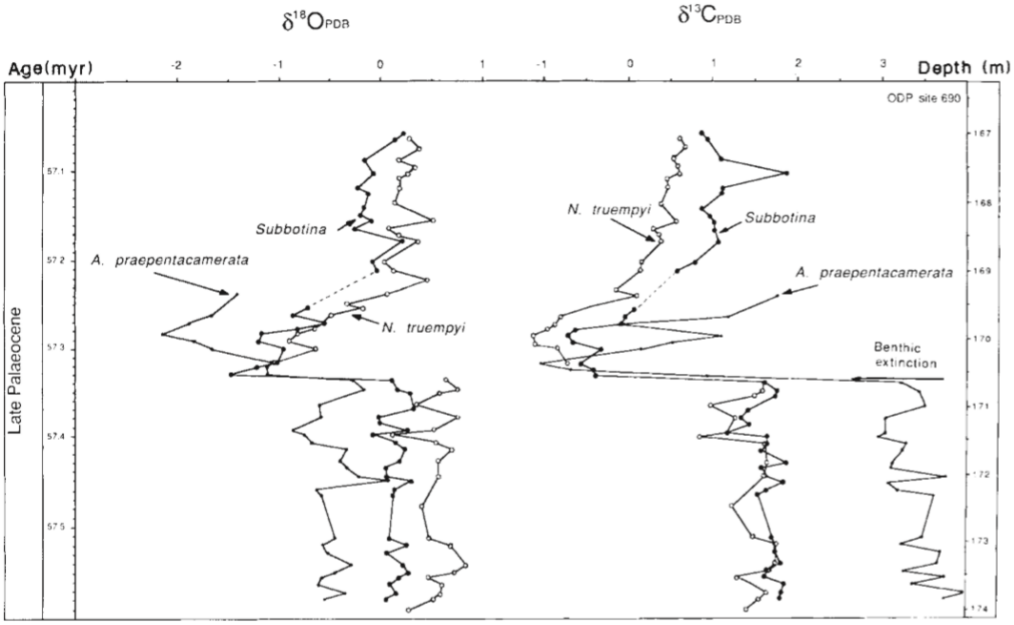

Figure 1: $^{18}O/^{16}O$ and $^{13}C/^{12}C$ plotted across the PETM. This data is taken from site 113-690B near Antarctica. [Kennet & Stott, 1991]

Analyses of isotopic carbon in marine and terrestrial sediments also indicate a large 2.5‰ (parts per mille) decrease in $^{13}C/^{12}C$ ratio (known as a carbon isotope

excursion; CIE), which indicates a major disruption of the global carbon cycle [Kennet & Stott, 1991]. (See Figure 1). Therefore, it is hypothesized that an abrupt release of carbon dioxide (CO_2) and or methane (CH_4) into the atmosphere is responsible for the increased global temperatures for the next 10 to 30 thousand years [Dickens et al., 1997]. This global warming initiated an increased rate of evaporation, which increased in magnitude towards the tropics and this moisture was transported towards the polar regions. This increase in precipitation at the poles reduced the salinity in the Arctic ocean and a major reversal of ocean currents in the north Atlantic, which may have culminated in a deep ocean anoxic environment [Pagani et al., 2006; Zachos et al., 2005]. Although the Paleocene epoch is considered to have been ice free, global sea levels are expected to have risen due to the thermal expansion of water [Sluijs et al., 2006].

Due to the massive influx of carbon into the atmosphere and the changes that occurred due to the abrupt temperature rise, organisms were forced to adapt or go extinct. The fossil record describes both of these scenarios; benthic foraminifera experienced a mass extinction of roughly 35% to 50% of all species while planktonic foraminifera diversified and subtropical dinoflagelates appear to have migrated from the tropics to higher latitudes [Thomas, 1998]. Among planktonic calcifyers unusual forms appear; such as small, flattened planktonic foraminifera and asymmetrical coccoliths secreted by coccolithophores [Kahn & Aubry, 2004; Aubry et al., 2007]. In terrestrial habitats, many modern orders of mammal migrated into North America and Europe, dispersing most probably from Asia [Smith et al., 2006]. While many of these biological changes are well-documented in the geologic record, the actual mechanism(s) leading to the PETM is still up for interpretation and is hotly debated amongst the scientific community. The largest difficulty is describing a scenario that could suddenly implant approximately 10^{18} grams (about 1000 gigatons) of carbon into the environment [Carozza et al., 2011]. These ideas include; the release

of methane clathrates [Dickens et al., 1997], the eruption of a large kimberlite field (e.g., Patterson & Francis, [2013]), massive volcanic activity argued (e.g., Svensen et al., [2004]), and the impact of a comet [Kent et al., 2003].

It is hypothesized that the PETM may have occurred in two or more short, yet major hyperthermals. Archer et al. [2009] suggests the initial onset of the warming was on the order of 200 to 2,000 years, while Wright & Schaller [2013] indicated a much broader timescale of 750 to 30,000 years. Current PETM isotope models predict that an initial deposition of carbon and subsequent warming took place, raising ocean temperatures by approximately 3°C. This would have been followed by a more dramatic event which added lighter carbon into the environment. This, in turn, caused the CIE [Dickens et al., 1997; Carozza et al., 2011]. These models suggest that the mechanism that caused the CIE may not be responsible for the initial warming.

1.1 Release of Methane Clathrates

Methane clathrates form via crystallization or precipitation when methane travels up geologic faults and contacts the cold deep ocean [Hoffmann, 2006]. Methane clathrates are commonly found in the shallow ocean geosphere and form outcrops on the ocean floor [Hoffmann, 2006]. An abrupt discharge of this methane would greatly increase the Earth's global warming potential (GWP) which would increase global temperatures. It is hypothesized this could result in a positive feedback loop, releasing more methane and continuing the cycle [Kennett et al., 2003]. Recently, the methane clathrate hypothesis has gained traction; many hypothesize that the sudden release of this methane ice from beneath the ocean floor may be responsible for the CIE, as it is highly depleted in ^{13}C [Dickens et al., 1997]. Although the methane clathrate hypothesis could be responsible for the secondary effects of the PETM, the event that triggered the perturbation and subsequent release of the methane remains unclear. The triggering event has been hypothesized to be any number of

near instantaneous events such as the eruption of a large kimberlite field [Patterson & Francis, 2013], massive degassing from volcanic activity in the Atlantic [Storey, Duncan & Swisher, 2007; Svensen et al., 2004], and even an impactor [Kent et al., 2003].

1.2 Eruption of a Large Kimberlite Field

Kimberlite pipes are deep-origin volcanoes that form when a deep magma chamber, rich in magnesium and volatiles such as water and CO_2, is pushed towards the surface [Patterson & Francis, 2013]. As the magma makes its way upward, it begins to encounter lower pressures. Eventually the volatile compounds within the magma change phase to a gaseous state and violently expand. This rapid expansion results in a shallow supersonic eruption of volatile-rich compounds [Patterson & Francis, 2013]. After the discovery of the approximately 56 Ma kimberlite field, a cluster of many kimberlite pipes, in the Lac de Gras region of northern Canada, it was hypothesized by [Patterson & Francis, 2013] that the eruption of these pipes could be responsible for the initial massive deposition of carbon, via volatiles such as CO_2, into the atmosphere.

1.3 Volcanic Activity

Massive volcanism has also been suggested as a source of the PETM. As the North Atlantic continued to open, considerable volcanism would have taken place along the mid-Atlantic ridge and up into East Greenland [Storey, Duncan & Swisher, 2007]. During the PETM, Europe and North America were about 20% closer than they are today (see Figure 2). Simultaneously, the Caribbean plate was undergoing a significant amount of volcanism during a period of increased activity and may also be responsible for the disruption of oceanic currents [Bralower et al., 1997]. This disruption of oceanic currents may have lead to the previously described decimation of many benthic foraminifera. However, this massive degassing would be 200 times the

observed Paleocene background rate and there is no evidence of such abrupt intense volcanism ever occurring.

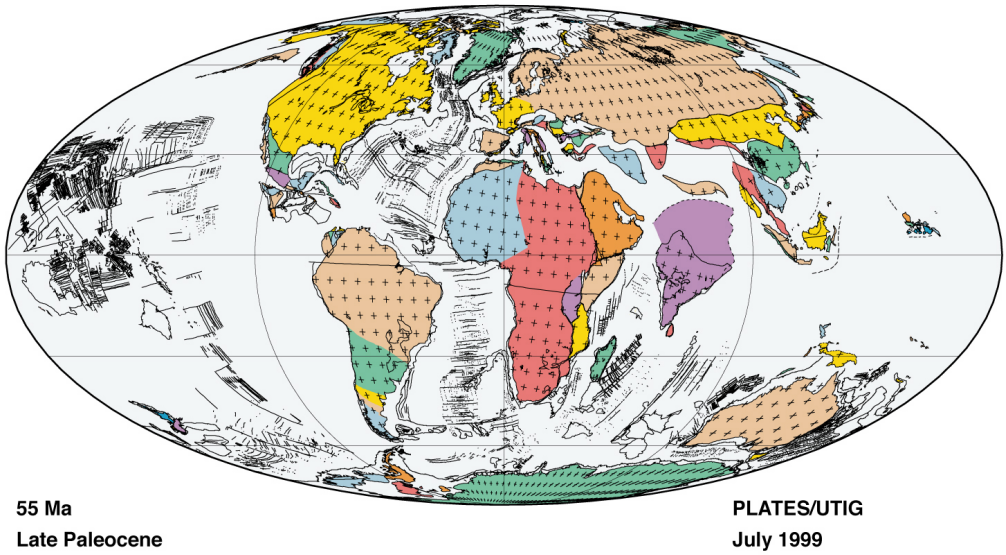

Figure 2: Paleogeographic reconstruction of Earth at 55 Ma [Lawver et al., 1999].

1.4 Impact

Ever since Alvarez [1980], suggested that an extraterrestrial impactor may have been responsible for the 66 Ma Cretaceous-Paleogene (K-Pg) extinction, impacts have been suggested for many instantaneous environmental and biological alterations recorded within the geologic record. It has been hypothesized that a ^{12}C-rich impactor slammed into the Earth at the onset of the PETM. This massive deposition of carbon may be responsible for the initial warming and the following carbon isotope excursion [Kent et al., 2003]. An impact can also explain several other features observed at the PETM boundary such as iridium anomalies in the Basque region of Spain, and the sudden emergence of single domain magnetite particles off the coast of New Jersey [Kent et al., 2003; Kent et al., 2017]. The largest hindrance to the impact hypothesis is the lack of an impact crater at the PETM. However the Chicxulub crater, hypoth-

esized to be responsible for the K-Pg extinction [Renne et al., 2013], occurred at a relatively shallow depth and was not properly identified until 1990 [Hildebrand et al., 1991]. Impacts occurring in deeper or less explored portions of the ocean may be more difficult to recognize.

1.5 Objectives

In this study, we assess to what extent impact induced changes to atmospheric chemistry could contribute to the onset of the PETM. First we calculate estimated greenhouse gas production by (1) combustion associated with forest fires [Collinson & Hooker 2003; Kent, 2017], (2) deposition of carbon from a carbon-rich impactor such as a carbonaceous chondrite or comet [Crovisier & Bockelée-Morvan, 1999], (3) deposition of water vapor, a greenhouse gas, from a water ice-rich carbonaceous chondrite or comet [Woods, et al., 1987], (4) the addition of vaporized crustal carbon deposits to the atmosphere, (5) the addition of water vapor to the atmosphere due to a deep oceanic impact [Toon & Lawless , 1994], and (6) NO formation and subsequent reactions resulting in formation of tropospheric ozone [Zahnle, 1990; Crutzen, 2003]. Below discuss how each of these mechanisms could contribute to climate forcing in more detail.

1.5.1 Fireball and Subsequent Greenhouse Gas Production

Although global forest fires have been rejected as the main cause of the PETM, there is still evidence pointing towards forest fires at the PETM boundary [Kent et al., 2017]. Forest fires could easily be ignited by a sufficiently large impact's fireball, as well as the globally re-entering ejecta. Assuming this fireball took place over a continent a sizeable portion of land would be scorched. This fire could then expand to a region much larger than the initial area consumed.

1.5.2 Deposition of Carbon via Carbonaceous Chondrite or Carbon-rich Cometary Impact

The most carbon-rich asteroids are known as C-type asteroids, or carbonaceous chondrites (when they land on Earth). These C-type asteroids are at most 5% carbon by mass [Pearson et al., 2006]. Comets are also known to contain CO_2 and CO ices along side a host of hydrocarbons, Crovisier and Bockelée-Morvan, [1999] suggest measurements as high as 15% carbon by mass comets.

1.5.3 Deposition of Water via Cometary or Water-rich Asteroidal Impact

Comets are inherently wet, although we do not have a statistically large data set to work with most comets appear to be approximately 40% water ice by mass [Woods, et al., 1987]. Some asteroids are also known to contain water, as evidenced by carbonaceous chondrite meteorites that contain as much as 17% water by mass [Jarosewich, 1990]. Upon impact, this water may be added to the Earth's hydrosphere as vapor.

1.5.4 Vaporization of Crustal Carbon Deposits due to Impact

Hunt [1972] determined that the total quantity of carbon contained in the Earth's crust was approximately 9×10^{22} g, if we assume an even distribution of this carbon throughout the crust, the impactor will vaporize some of this carbon. This carbon will then join the atmosphere and have a chance to bond with free O_2 forming CO_2.

1.5.5 Vaporization of Water due to an Oceanic Impact

Assuming the impactor strikes the deep ocean (the most probable location for an impact, as oceans cover 71% of the Earth's surface) large amounts of ocean water will be vaporized. A much larger volume of ocean will be displaced than the mass of the impactor [Toon & Lawless , 1994]. This water vapor will be ejected high into the

atmosphere and act as a greenhouse gas.

1.5.6 NO Production and Subsequent O_3

When large amounts of energy are absorbed by the atmosphere, such as by lightning strikes or impactors, the main constituents of the atmosphere, 22.5% diatomic oxygen (O_2) and 77.5% diatomic nitrogen (N_2), gain enough energy to dissociate and become monatomic oxygen (O) and monatomic nitrogen (N). This dissociation occurs at roughly 1700 K and once these atoms drop below this temperature they begin to recombine. The vast majority of these recombinations results in O_2 and N_2 however a small percentage of NO also forms. NO by itself is not a greenhouse gas but when combined with water vapor in the atmosphere it can be rained out as nitric acid (HNO_3) which can be devastating to the environment [Holleman & Wiberg, 2001]. Furthermore this NO readily bonds with and destroys ozone, but ultimately contributes to the re-deposition of ozone in the troposphere where this ozone may act as a powerful greenhouse gas roughly 69 times as potent as CO_2 [Kiehl et al., 1997]

2. Methods

In this study, we explore chemical changes made to the bulk atmosphere induced by impactors with radii of 2.5 km and 5 km. These sizes are in agreement with hypothetical PETM impactors proposed by workers such as Kent [2003]. For each impactor size, we calculated greenhouse gas production for both cometary and asteroidal impacts. We assumed a cometary density of 0.6 g/cm^3 [Britt et al., 2006] and an asteroidal density of 2.865 g/cm^3 as previously utilized by Zahnle [1990] for a K-Pg impactor. For simplicity, we assumed all impacts were perpendicular to the Earth surface; this results in a minimum energy deposition and is discussed in greater detail in Section 4. For asteroids, we assumed a maximum velocity of 17 km/s and minimum velocity of 11 km/s proposed by Collins et al. [2005]. For comets we used velocities of 51 km/s and 72 km/s for our lower and upper bounds [Collins et al., 2005]. For each impactor we investigated two options for the target material: (1) a lithosphere with density of 2.9 g/cm^3 [Silver & Schultz, 1982] and (2) a 3.688 km deep ocean with an average density of 1.028 g/cm^3 overlying lithospheric material with density 2.9 g/cm^3 [Central Intelligence Agency, 2018]. For reference, comprehensive lists of our constants and variables are provided in Table 14 and Table 15 of the Appendix (Section 6).

2.1 Fireball and Subsequent Release of Biogenic Carbon

Here we assume an average land cover of biogenic carbon (e.g., plants, bacteria, fungi, animals, protists, archaea, viruses, etc.) over all land area and multiply that by the fractional area of land encompassed within the impact fireball [Bar-On et al., 2018; Weast & Robert, 1968].

$$M_c = \pi R_{fb}^2 \frac{M_{bc}}{A_c} \tag{2.1}$$

where R_fb is the radius of the fireball, determined via the Impact Earth online simulator [Collins et al., 2005], M_{bc} is the total mass of biogenic carbon on land, here we

assume the mass of biogenic carbon is mostly on land, as trees make up 90% of this value Bar-On et al. [2018], and A_c represents the Earth's total land area [Central Intelligence Agency, 2018]. In the unlikely event that all of this carbon were to bond with oxygen and form CO_2, the resulting yield of CO_2 would be:

$$M_{CO_2} = \frac{2m_O + m_C}{m_C} M_c \tag{2.2}$$

where m_C is the mass of a carbon atom and m_O is the mass of an oxygen atom.

2.2 Impact Deposition of Carbon

Comets are rich in CO_2 and CO ices along with hydrocarbons such as CH_4, CH_3OH, and H_2CO among others. The total mass of carbon in a typical comet such as Hale-Bopp can be as large as 15% [Crovisier, & Bockelée-Morvan, 1999]. Adopting this constraint, we assume:

$$M_c = 0.15 M_i \tag{2.3}$$

where M_c is the impactor's total mass of carbon contained within the impactor, and M_i is the impactor's total mass.

C-type asteroids are the most carbon-rich of all asteroids. As discussed above, they may contain up to 5% carbon by mass. Therefore, we assume:

$$M_c = 0.05 M_i \tag{2.4}$$

Although comets can have a larger percentage of carbon contained within them, their low density means an asteroid of similar size will contain more carbon overall.

2.3 Impact Deposition of Water Vapor

Comets are approximately 40% water ice by mass [Woods, 1987]. Therefore, we assume:

$$M_w = 0.4 M_i \tag{2.5}$$

where M_w is the impactor's total mass of water, and M_i is the impactor's total mass.

A study conducted by Jarosewich [1990] states that carbonaceous chondrites can be as much as 17% water by mass. Therefore, we assume:

$$M_w = 0.17 M_i \tag{2.6}$$

Water vapor is a powerful greenhouse gas on short time scales, but on longer time scales its GWP drops significantly. Over 100 years (which allows for water to equilibrate in the atmosphere), the GWP of water vapor is at most 5×10^{-4} of CO_2 [Sherwood et al., 2018]. Therefore, the mass of CO_2 required to produce the equivalent climate forcing would be:

$$M_{EQ_{CO_2}} = 5 \times 10^{-4} M_w \tag{2.7}$$

Although comets are composed of a larger percentage of water, the most water-rich asteroids may contain twice as much water due to their higher density.

2.4 Vaporization of Crustal Carbon

The Central Intelligence Agency [2018] estimates that 71% of the Earth surface is covered by ocean, leaving 29% of the surface covered by continents. We will use this data as a proxy for what percentage of the surface is covered by oceanic and continental crust. Monroe & Wicander [2001] state that the average continental crust thickness is approximately 35 km, while the average oceanic crust ranges from 5 to 10 km thick, we will assume an average oceanic crust thickness of 7.5 km. We will then find the average thickness of the entire crust by weighting each thickness by the amount of Earth's surface they each cover.

$$d_C = (0.29\, d_{cc}) + (0.71\, d_{oc}) \tag{2.8}$$

where d_C is the average weighted crustal thickness, d_{cc} is the average continental crustal thickness, and d_{oc} is the average oceanic crustal thickness.

To determine the the total volume occupied by the crust we do the following:

$$V_C = \frac{4}{3}\pi[R^3 - (R - d_C)^3] \tag{2.9}$$

where V_C is the total volume occupied by Earth's crust and R is the Earth's radius.

Hunt [1972] determined that the total amount of Earth carbon contained in the Earth's crust was approximately 9×10^{22} g,thus the average density of carbon within the Earth's crust is just:

$$\rho_c = \frac{M_{CC}}{V_C} \tag{2.10}$$

where ρ_c and M_{CC} are the average mass density and the total mass of carbon contained within the Earth's crust respectively.

We then take this density and divide it by the average density of the Earth's crust, ρ_t, to get the average number density of carbon, n_c, held within the Earth's crust:

$$n_c = \frac{\rho_c}{\rho_t} \tag{2.11}$$

Finally we multiply the total mass of rock vapor ejected via the impact by ρ_c. To first order this will give us the total mass of carbon ejected from the crust and deposited into the atmosphere by a large impact.

$$M_c = n_c\, M_v \tag{2.12}$$

where M_c and M_v are the total mass of carbon and the total mass of rock vapor ejected by the impact respectively.

Due to the scale of these impacts, oceanic impacts due not deviate much from continental impacts, thus we will not discriminate them in Table 4.

2.5 Vaporization of Ocean Water

For simplicity, we assume that all of the kinetic energy lost from the impactor traveling through an ocean is gained by the water as random thermal energy. Thus,

$$KE_{Lost} = \frac{1}{2}\delta M_i v_i^2 \tag{2.13}$$

where KE_{Lost} is the kinetic energy lost from the impactor and gained by the ocean, δM_i is the mass lost, due to ablation, by the impactor as it travels perpendicularly through the ocean, and v_i is initial velocity of the impactor and its constituent parts (note: we are assuming the impactor does not slow down while traveling through the ocean). Therefore,

$$M_w = \frac{KE_{Lost}}{Q_{sw}} \tag{2.14}$$

where M_w is the mass of water vaporized and Q_{sw} is the latent heat of vaporization of sea water [Hunter & Harding 2002].

2.6 NO and Resulting O_3 Production

NO Production due to impacts can be divided into three parts; primary, secondary, and tertiary production. Primary production of NO is due to the hypervelocity impactor shocking a column of atmosphere, assumed here to be a mixture of 22.5% O_2 and 77.5% N_2 (note these values differ slightly from present day values) at 55.8 Myr [Hildebrand et al., 1991]. Additionally for simplicity we assume purely perpendicular impacts. This assumption will have little effect on the overall NO production for large impacts, but due to the smaller atmospheric path length it will result in the minimum NO production for a given impactor [Zahnle, 1990]. If the impactor is small enough it will deposit all of its energy into the atmosphere in this stage, resulting in an airburst.

Secondary production takes place after the impactor has contacted with the ground, here we assume the entire mass of the remaining impactor has been vaporized and the ejected target volume is dependent on the ratio of the densities of the impactor and target respectively [Zahnle, 1990]. This mass of material is then ejected in a cone

originating from ground zero. This cone of ejecta then shock heats the atmosphere, again causing more NO production. Some of this material is shock heated to energies large enough that widespread atmospheric escape occurs - this material occurs in a smaller cone also centered at the impact site and the volume of shocked atmosphere is not included in the total NO production [Zahnle, 1990]. More energetic impacts result in a more voluminous cone of ejecta and escaped material. At infinite energy, both cones would be approximated as planes ($\theta = 90°$) and all material in that volume would be ejected from the atmosphere entirely, leading to no NO production.

Both primary and secondary production of NO yield local concentrations. However, tertiary production affects global concentrations [Zahnle, 1990]. Tertiary production of NO occurs when this ejected material begins to re-enter Earth's atmosphere at near-orbital velocities. This material can later be broken down into different types of ejecta (i.e., the ejecta blanket, spalls and condensates) that react with the atmosphere. This material then shock heats the upper atmosphere globally and further produces NO [Zahnle, 1990]. Methods for estimating NO production are described in detail in the Appendix (Section 6).

2.7 Total GWP due to Impactor

Here we simply add up each contributing mechanism in terms of GWP in order to determine the total GWP. For continental impacts we add up GWP from O_3, biogenic carbon and the chemical make-up of the impactor. For an oceanic impact we sum the GWP from the O_3, the chemical make-up and the amount of vaporized water.

2.8 CO_2 - Temperature Relation

From Myhre et al., [1998]

$$\Delta T = 10.29\, ln\left[\frac{n_{CO_2}}{n_0}\right] \tag{2.15}$$

where n_{CO_2} is the atmospheric concentration of CO_2 and n_0 is a known reference CO_2 value from Berner [1990].

We will convert our known GWP into a number density by dividing it by the total mass of the atmosphere.

3. Results

3.1 Continental Fireball

In this section, we summarize the effects of fireball-induced combustion for impacts occurring on land. Fireball size has a direct relationship with kinetic energy. Therefore, the less massive yet significantly more energetic comets produce a larger fireball irrespective of impactor size. Fireball sizes for our impacts range from 45 km to 186 km in radius. Assuming all impacts occur in a typical density region of biogenic carbon, we would release 6.79×10^{11} g to 6.52×10^{12} g of carbon into the environment [Table 1]. We then make the (unlikely) assumption that nearly all of this carbon would immediately encounter an O_2 molecule and produce CO_2. However, as discussed below, this mass of CO_2 is insignificant compared to our other sources. For our most energetic impacts, this corresponds to approximately 10^{13} grams of CO_2 released, which is five orders of magnitude less than required to initiate the warming. The amount of carbon produced by combustion could be smaller or larger depending on the location of the impact, (i.e., hitting a desert versus a tropical rain forest). Additionally, it should be noted these fires may have spread well beyond the initial radius covered by the fireball so our values should be considered as a lower bound.

Table 1: Biogenic Carbon released via Fireball

Object	Radius [cm]	Radius of Fireball [cm]	Min C [g]	Max C [g]
Asteroid	2.5×10^5	4.50×10^5 - 6.00×10^5	6.79×10^{11}	1.21×10^{12}
Asteroid	5.0×10^5	9.00×10^5 - 1.20×10^6	1.53×10^{12}	2.71×10^{12}
Comet	2.5×10^5	7.40×10^5 - 9.30×10^5	1.03×10^{12}	1.63×10^{12}
Comet	5.0×10^5	1.48×10^6 - 1.86×10^6	4.10×10^{12}	6.52×10^{12}

3.2 Carbon-rich Impactor

We set an upper and lower limit on the amount of carbon being carried by asteroids and comets. Although comets hold a larger percentage of the mass in carbons

(mainly hydrocarbons, CO_2 and CO-ices) their lower mass compared to their relatively carbon-poor asteroid counterparts results in asteroids carrying more carbon overall. For our lower limit we assume the comet and or asteroid has zero carbon content (an unlikely assumption, but a robust lower limit) and our maximum contents were determined via observations from comets such as Hale-Bopp and carbon-rich asteroids and carbonaceous chondrite meteorites. The maximum insertion of carbon into the atmosphere would be between 5.89×10^{15} g to 7.50×10^{16} g of carbon [Table 2]. Assuming this deposited carbon immediately bonds with an O_2 molecule, it would result in a maximum mass of 2.15×10^{16} g to 2.73×10^{17} g of CO_2. Although this input of CO_2 may not be enough to explain the initial warming on its own, the vaporization and deposition of a C-type asteroid into the atmosphere could be a contributing factor to the global temperature rise.

Table 2: Impactor Deposition of Carbon and CO_2 Production

Object	Radius [cm]	Max C [g]	Max CO_2 [g]
Asteroid	2.5×10^5	9.38×10^{15}	3.42×10^{16}
Asteroid	5.0×10^5	7.50×10^{16}	2.73×10^{17}
Comet	2.5×10^5	5.89×10^{15}	2.15×10^{16}
Comet	5.0×10^5	4.73×10^{16}	1.72×10^{17}

3.3 Water-rich Impactor

We set an upper and lower limit on the amount of water being carried by asteroids and comets. Although comets hold a larger percentage of the mass in water-ice and water bearing minerals, their lower mass compared to their relatively water-poor asteroid counterparts results in asteroids carrying more water overall. For our lower limit we assume the comet and or asteroid has zero water content (an unlikely assumption, but a robust lower limit) and our maximum contents were determined via observations from comets such as Hale-Bopp and water-rich asteroids (carbonaceous chondrites). The maximum insertion of carbon into the atmosphere would be between

1.57×10^{16} g to 2.55×10^{17} g of water [Table 3]. We then take this maximum water content and multiply it by its long term, 100 years, GWP of 5×10^{-4} to determine the equivalent production of CO_2. The resulting maximum equivalent production of CO_2 ranges from 7.85×10^{12} g to 1.285×10^{14} g. Assuming the 100-year GWP for water, the mass of water added to the hydrosphere via extraterrestrial origin would be four orders of magnitude less than required to explain the initial warming event.

Table 3: Impactor Deposition of H_2O and Equivalent CO_2 Production

Object	Radius [cm]	Max H_2O [g]	Max CO_2 [g]
Asteroid	2.5×10^5	3.19×10^{16}	1.59×10^{13}
Asteroid	5.0×10^5	2.55×10^{17}	1.28×10^{14}
Comet	2.5×10^5	1.57×10^{16}	7.85×10^{12}
Comet	5.0×10^5	1.26×10^{17}	6.28×10^{13}

3.4 Vaporized Crustal Carbon Deposits

Larger impacts vaporize a larger volume of crustal rock and produce a larger plume of vaporized rock. The size of the column of vaporized rock is directly related to the amount of kinetic energy deposited into the ocean. Analogous to the fireball production, the less massive yet significantly more energetic comets vaporize more rock than asteroids of the same radii. Assuming all impacts occur in a typical region of Earth's crust, containing on average 0.389% carbon by volume, they would vaporize between 9.26×10^{14} g to 3.04×10^{16} g of carbon [Table 4]. Assuming this ejected carbon immediately bonds with an O_2 molecule, it would result in a maximum mass of 3.39×10^{15} g to 1.11×10^{17} g of CO_2. Although this input of CO_2 may not be enough to explain the initial warming on its own, the vaporization of a typical region of crustal carbon deposits into the atmosphere could be a contributing factor to the global temperature rise.

Table 4: Mass of Vaporized Carbon Ejecta

Object	Radius [cm]	C [g]	CO_2 [g]
Asteroid	2.5×10^5	9.26×10^{14}	3.39×10^{15}
Asteroid	5.0×10^5	7.41×10^{15}	2.71×10^{16}
Comet	2.5×10^5	3.96×10^{15}	1.45×10^{16}
Comet	5.0×10^5	3.04×10^{16}	1.11×10^{17}

3.5 Vaporized Ocean Water

Larger impacts vaporize a larger volume of ocean and a larger plume of water vapor. The size of the column of vaporized water is directly related to the amount of kinetic energy deposited into the ocean. Analogous to the fireball production, the less massive yet significantly more energetic comets vaporize more water than asteroids of the same radii. In fact, the minimum for a small comet is more than that of the maximum for the largest asteroid. This unexpected result is due to the significantly smaller ablation coefficient of ice compared to that of rock. Having a smaller ablation coefficient allows the comet to deposit more of its energy into the ocean and atmosphere. Assuming all impacts occur in a typical deep region of the ocean we would vaporize between 3.09×10^{18} g to 2.44×10^{20} g of water [Table 5]. To put this into prospective, a 10 km diameter comet could vaporize nearly 11 times the volume of the Great Lakes combined, and this is an outcome of the minimizing assumption of an impact perpendicular to the surface.

Table 5: Mass of Water Vapor produced

Object	Radius [cm]	Min H_2O [g]	Max H_2O [g]
Asteroid	2.5×10^5	3.09×10^{18}	7.38×10^{18}
Asteroid	5.0×10^5	1.24×10^{19}	2.95×10^{19}
Comet	2.5×10^5	3.06×10^{19}	6.09×10^{19}
Comet	5.0×10^5	1.22×10^{20}	2.44×10^{20}

We take these water vapor outputs and multiply them by the 100 year GWP for

water to determine the equivalent production of CO_2. Following the same trends as before (i.e., comets produce significantly more water vapor than asteroids) we determine that this is equivalent to the deposition of 1.55×10^{15} g and 1.22×10^{17} g of CO_2 into the atmosphere [Table 6]. By itself, vaporization of water vapor cannot account for the total initial temperature rise of the PETM. However, it could be a major contributor and should not be neglected in the case of an oceanic impact.

Table 6: GWP Equivalent of CO_2 Production via H_2O

Object	Radius [cm]	Min CO_2 [g]	Max CO_2 [g]
Asteroid	2.5×10^5	1.55×10^{15}	3.69×10^{15}
Asteroid	5.0×10^5	6.22×10^{15}	1.48×10^{16}
Comet	2.5×10^5	1.53×10^{16}	3.05×10^{16}
Comet	5.0×10^5	6.10×10^{16}	1.22×10^{17}

3.6 Total NO and Subsequent O_3 Production

Here we summarize the total atmospheric production of NO via all eight impact scenarios considered. Larger impacts produce more NO and comets tend to generate more NO than asteroids. Additionally, continental impacts produce slightly more NO than oceanic impacts, which agrees with the results produced by Zahnle [1990]. Our results for NO production ranged from 4.06×10^{14} g to 1.21×10^{18} g [Table 7]. Our largest NO production is equivalent a 0.08% by volume atmospheric concentration.

Table 7: NO Production via Impacts

Object	Radius [cm]	Site	Min NO [g]	Max NO [g]
Asteroid	2.5×10^5	Continent	4.06×10^{14}	4.93×10^{15}
Asteroid	2.5×10^5	Ocean	4.01×10^{14}	4.70×10^{15}
Asteroid	5.0×10^5	Continent	3.03×10^{15}	3.82×10^{16}
Asteroid	5.0×10^5	Ocean	2.77×10^{15}	3.38×10^{16}
Comet	2.5×10^5	Continent	5.35×10^{16}	2.80×10^{17}
Comet	2.5×10^5	Ocean	4.69×10^{16}	2.62×10^{17}
Comet	5.0×10^5	Continent	2.53×10^{17}	1.21×10^{18}
Comet	5.0×10^5	Ocean	2.24×10^{17}	1.11×10^{18}

For our O_3 production, NO is still the limiting reactant for our 2.5 km radius minimum cases, for all other cases the global CO reservoir is the limiting molecule. This CO limit is attributable to the first reaction in the NO to O_3 reaction series (see Section 6, Appendix); this reaction requires CO, and all subsequent reactions require molecules which occur at higher concentrations in our atmosphere. Because of this, the global CO concentration effectively creates a ceiling for maximum NO production. If global CO levels during the Late Paleocene were larger than present day natural levels, all of these plateaued values would rise as well. Due to this CO ceiling, any global NO production greater than 80 ppb (parts per billion) is omitted from our calculations. Our resulting O_3 values range from 4.01×10^{14} g to 4.12×10^{14} g of O_3 [Table 8].

Table 8: O_3 Production via Impacts

Object	Radius [cm]	Site	Min O_3 [g]	Max O_3 [g]
Asteroid	2.5×10^5	Continent	4.06×10^{14}	4.12×10^{14}
Asteroid	2.5×10^5	Ocean	4.01×10^{14}	4.12×10^{14}
Asteroid	5.0×10^5	Continent	4.12×10^{14}	4.12×10^{14}
Asteroid	5.0×10^5	Ocean	4.12×10^{14}	4.12×10^{14}
Comet	2.5×10^5	Continent	4.12×10^{14}	4.12×10^{14}
Comet	2.5×10^5	Ocean	4.12×10^{14}	4.12×10^{14}
Comet	5.0×10^5	Continent	4.12×10^{14}	4.19×10^{14}
Comet	5.0×10^5	Ocean	4.12×10^{14}	4.12×10^{14}

Taking our previous range of O_3 and multiplying it by its 100-year GWP of approximately 69 we can determine the equivalent production of CO_2. We determined that the maximum equivalent production of CO_2 ranges from 2.21×10^{16} g to 2.84×10^{16} g [Table 9].

Table 9: GWP Equivalent of CO_2 Production via O_3

Object	Radius [cm]	Site	Min CO_2 [g]	Max CO_2 [g]
Asteroid	2.5×10^5	Continent	2.80×10^{16}	2.84×10^{16}
Asteroid	2.5×10^5	Ocean	2.21×10^{16}	2.84×10^{16}
Asteroid	5.0×10^5	Continent	2.84×10^{16}	2.84×10^{16}
Asteroid	5.0×10^5	Ocean	2.84×10^{16}	2.84×10^{16}
Comet	2.5×10^5	Continent	2.84×10^{16}	2.84×10^{16}
Comet	2.5×10^5	Ocean	2.84×10^{16}	2.84×10^{16}
Comet	5.0×10^5	Continent	2.84×10^{16}	2.84×10^{16}
Comet	5.0×10^5	Ocean	2.84×10^{16}	2.84×10^{16}

3.7 Total GWP and Subsequent Temperature Rise

Our minimum values for asteroids tend to stay near the hypothetical CO ceiling created by reactions converting NO to O_3 to GWP CO_2. This is due to the limited addition of CO_2 from the fireball and zero addition from any other sources. Our maximum values for asteroids grow quite a bit due to their addition more C and H_2O composition. On average oceanic impacts create the most CO_2 due to their contribution from vaporized water out weighing their lack of continent based biogenic carbon. After totaling up our GWP equivalent CO_2 values and our raw CO_2 values, we determined that the equivalent mass range of deposited CO_2 is 2.55×10^{16} g to 4.33×10^{17} g [Table 10].

Table 10: Total GWP Equivalent of CO_2

Object	Radius [cm]	Site	Min CO_2 [g]	Max CO_2 [g]
Asteroid	2.5×10^5	Continent	3.14×10^{16}	6.60×10^{16}
Asteroid	2.5×10^5	Ocean	2.55×10^{16}	6.97×10^{16}
Asteroid	5.0×10^5	Continent	6.17×10^{16}	3.29×10^{17}
Asteroid	5.0×10^5	Ocean	6.17×10^{16}	3.43×10^{17}
Comet	2.5×10^5	Continent	4.29×10^{16}	6.44×10^{16}
Comet	2.5×10^5	Ocean	5.82×10^{16}	9.49×10^{16}
Comet	5.0×10^5	Continent	5.88×10^{16}	3.11×10^{17}
Comet	5.0×10^5	Ocean	2.00×10^{17}	4.33×10^{17}

The results for the expected initial temperature rise due to impacts of various sizes and compositions are described below. Our global temperature increases are directly related to the log of the atmospheric equivalent CO_2 deposition. Here we have determined that we would expect a rise of 0.34°C to 4.69°C [Table 11].

Table 11: Total Temperature Rise due to Impact

Object	Radius [cm]	Site	ΔT_{Min}	ΔT_{Max}
Asteroid	2.5×10^5	Continent	0.42°C	0.86°C
Asteroid	2.5×10^5	Ocean	0.34°C	0.91°C
Asteroid	5.0×10^5	Continent	0.81°C	3.72°C
Asteroid	5.0×10^5	Ocean	0.81°C	3.83°C
Comet	2.5×10^5	Continent	0.57°C	0.84°C
Comet	2.5×10^5	Ocean	0.76°C	1.22°C
Comet	5.0×10^5	Continent	0.77°C	3.55°C
Comet	5.0×10^5	Ocean	2.42°C	4.69°C

4. Discussion

In this work, we determined that perpendicular impacts of comets with radii of 5 km may result in global warming of up to 4.69°C. However, this value may represent either an underestimate or overestimate of the actual value, depending on both the initial conditions assumed in our calculations as well as other effects that were not incorporated into our calculations. In this section, we summarize the uncertainties associated with our results. Then, we discuss a number of factors that more broadly may provide arguments for or against an impact trigger for the PETM.

Many of our initial conditions resulted in underestimates of impact-induced global warming. For example, oblique impacts would lead to significantly larger amounts of vaporized water in the case of an oceanic impact and biogenic material in the case of a continental impact [Zahnle, 1990]. Zahnle [1990] states the maximum amount of energy that can be deposited into the ocean is when the impactor encounters its own mass in water. To first order, a 5 km radius comet colliding with the ocean at an angle of 20° (45° is the average impact angle) from horizontal would vaporize approximately five times as much water and result in a global temperature rise of approximately 7°C, far more than required to explain the initial warming. This value was determined by calculating the mass of water encountered by the impactor compared to a perpendicular impact and giving all of its energy to the surrounding ocean. Another limiting assumption was that the region burned by the fireball was the only source of biogenic carbon and that the fires did not spread beyond the fireball's initial radius. Additionally, much of the ejected material raining down across the planet could also generate powerful wildfires [Collinson & Hooker 2003; Kent, 2017]. Subsequently, this area need not be a single connected region, leading to the difficulty of its discovery. Another plausible scenario neglected in this study would be, in the case of an oceanic impact, if the impactor directly struck a methane clathrate deposit or another especially carbon-rich region. The effects due to the impactor

combined with the massive release of methane from a large clathrate deposit could be responsible for the initial warming, and could eventually cause the release of further global deposits causing further temperature rise and the CIE.

We also had many assumptions that may have led to overestimates of global warming. In our study we attempted to determine a maximum production of GWP equivalent of CO_2. Thus, we neglected the effects of dust, clouds and some complicated chemical effects. During an impact, dust is ejected far into the upper atmosphere and can stay suspended for months, years or even decades [Zahnle, 1990; Artemieva et al., 2017]. This dust blocks solar radiation from reaching the surface and a resulting cooling effect is created. Similarly, the rapid vaporization of water may result in the formation of clouds. Clouds are complicated to model and may result in warming or cooling effects. Because of this complicated relationship with water and climate forcing, there has been much debate in determining water's true GWP [Sherwood et al., 2018]. Sherwood et al. [2018] estimates the long term GWP of water to between -10^{-3} (a negative GWP denotes a global coolant) and 5×10^{-4}. Furthermore, our calculations assumed that all of the atmospheric carbon from the release of biogenic sources and deposited sources from the impactor themselves immediately bound to atmospheric O_2 rather than being trapped in natural sinks such as exposed rock and the oceans. Additionally, once this carbon was bound up in CO_2 we ignored the effect of carbon sequestration by these natural sinks as well. Similarly, we made the assumption that all CO molecules in the atmosphere would be consumed by the NO reaction sequence and that it would operator at maximum efficiency. Other causes for a misrepresentation of realistic effects include our decision to use the 100-year GWP value. As previously stated, Archer et al. [2009] suggests the initial onset of the warming was on the order of 200 to 2000 years, while Wright & Schaller [2013] indicated a much broader timescale of 750 to 30,000 years. As such, it is unclear what the most appropriate GWP timescale would be. In general, determining the event that

produced the initial onset of the PETM is further complicated by the approximately 1000 year incorporation time of organic matter [Mollenhauer et al., 2005].

A known point of comparison to the hypothesized PETM-triggering impact is the 66 Ma Chicxulub impact. Because the K-Pg extinction event is marked with a noticeable dip in global temperatures, the question arises as to how an impact could produce a net global warming effect. A key difference between the Chicxulub impact and a hypothetical PETM impactor is that the K-Pg impactor struck a massive gypsum deposit releasing an estimated 3×10^{17} g of sulfur into the atmosphere [Artemieva et al., 2017]. This sulfur then bonded with O_2 to form SO_2 a global coolant which both absorbs and backscatters solar radiation which in turn causes a rapid cooling effect near the surface [Artemieva et al., 2017]. This SO_2 paired with the previously mentioned light reflecting dust resulted in a short term cooling effect that trumped what would have been global increase in temperature.

The Chicxulub impact is known to have produced a gigantic tsunami. However, after an exhaustive literature search we were unable to find any documented evidence of tsunamis along the coastlines at the onset of the PETM. Whether this is evidence of a lack of an oceanic impact or a lack of investigative work at the onset of the PETM is yet to be determined. Vaporization of massive amounts of ocean water would have also produced sea level changes in both the Chicxulub and the hypothesized PETM impacts. In the case of our largest oceanic impacts, we calculated that on the order of 10^{20} g of water would be vaporized from the ocean. This massive loss of water would result in a global sea level drop, this appears to agree with observations made by Schmitz & Pujalte [2003]. Removing 2.44×10^{20} g of water from a reservoir of 1.41×10^{24} would result in a sea level drop of 0.635 m. There may also be a drop in sea level due to the loss of ejected rock vapor as well. This line of evidence appears to match up with Schmitz & Pujalte [2003]. Schmitz & Pujalte [2003] state that during the onset of the PETM there appears to be a prominent sea level lowstand.

Unfortunately the precise sea level drop has yet to be determined.

Finally, in most prior discussions of the PETM impact hypothesis it is assumed that the CIE is directly linked to the impactor rather than the accumulative effects of the impact over a longer duration of time [Kent, 2003]. Normally a ^{12}C-rich impactor is invoked to explain the CIE. However, a major issue with this model is the extent of time between the initial temperature rise and the onset of the CIE [Archer et al., 2009]. As discussed previously, it is currently hypothesized that the PETM may have occurred in two or more short, yet major hyperthermals. However, if the impactor was not enriched in ^{12}C this could allow the planet to warm due the effect of the impact (the first hyperthermal) and eventually release massive methane clathrate formations along the ocean floor. The release of methane clathrates is one of the current major hypotheses of the CIE (the second hyperthermal), and fits neatly into an impact narrative [Dickens et al., 1997].

5. Conclusion

In this work, we calculated the 100-year GWP equivalent CO_2 production and accompanying temperature rise corresponding to various impact-induced changes in atmospheric chemistry that may have accompanied a hypothetical impact timed to the onset of the PETM. In this study, we included biogenic carbon that would be released from a region consumed by the impact fireball. Then we considered carbon deposited directly by the impactor and the total mass of water vapor that could be deposited into the atmosphere from vaporization of the impactor. We determined the amount of carbon which would be released from a typical region of crust and in the case of an oceanic impact, the total mass of ocean water vaporized by the impactor. We then determined the amount of NO generated in the atmosphere via passage of a large hyper velocity impactor and subsequent chemical reactions resulting in the production of tropospheric O_3. With all these effects combined, many of our impactors were unable to reach the 5°C rise in temperatures observed at the PETM onset, however our maximum results for a perpendicular oceanic impact of a 5km comet came very close. We believe that a 4.69°C rise may be within error of the observed 5°C rise. However, we acknowledge these values are based on assumptions that may yield underestimated or overestimated global warming effects. As such, further work is needed to better understand the climatic effects of large impact events.

6. Appendix

We used the approach of Zahnle [1990] to calculate the primary, secondary, tertiary and total NO production. Afterwards, we calculated the production of tropospheric ozone following the approach demonstrated by Crutzen [2003].

6.1 Primary Production of NO

Using Zahnle's assumed freeze out temperature $T = 1700$ K for a similar sized K-Pg impactor, we can begin to calculate how much of the atmosphere is converted into NO. For this we require the equilibrium reaction rate, which are presented in Table 12 [Zahnle, 1990].

Table 12: Equilibrium Constant

Symbol	Reaction	Equation
K_1	$O_2 \rightarrow O + O$	$N_A\left[28.74 - \frac{T(K)}{380} + \left(\frac{T(K)}{3180}\right)^2\right] e^{-\frac{59500}{T(K)}}$
K_2	$N_2 \rightarrow N + N$	$N_A\left[21.32 - \frac{T(K)}{810} + \left(\frac{T(K)}{3020}\right)^2\right] e^{-\frac{113000}{T(K)}}$
K_3	$NO \rightarrow N + O$	$N_A\left[6.1 - \frac{T(K)}{1960} + \left(\frac{T(K)}{5800}\right)^2\right] e^{-\frac{75500}{T(K)}}$
K_4	$NO + O \rightarrow N + O_2$	K_3/K_1
K_5	$N_2 + O \rightarrow NO + N$	K_2/K_3

Once we have our K-values we can use the following relation to solve for the fraction of atmosphere that is converted to NO via shock.

$$f_{NO}(T) = \left(f_{N_2} f_{O_2} \frac{K_1 K_2}{K_3^2}\right)^{1/2} \tag{6.1}$$

where f_{N_2} and f_{O_2} are the fraction of the atmosphere that is N_2 and O_2 respectively. Now we can solve for the net yield of NO created as the impactor passes through the atmosphere.

For impactors large enough to survive entry into the atmosphere and contact the ground:

$$N_{NO_P} = \frac{(\gamma - 1)}{k_b T} f_{NO}(T) \frac{P}{g} \Gamma \pi r^2 v_i^2 \left(1 + \frac{\sigma}{2} v_i^2\right) \tag{6.2}$$

where γ is the gas constant at temperature T, k_b is the Boltzmann constant, P is the initial surface atmospheric pressure at sea level, g is the acceleration due gravity, Γ is the drag coefficient, r is the radius of the impactor, v_i is the initial velocity of the impactor and σ is the ablation parameter. The ablation parameter is inversely proportional to the latent heat of vaporization of the material (i.e., an icy body will have a larger ablation coefficient than a rocky one.) [Zahnle, 1990]

To determine the total mass of NO produced during primary production we simply multiply the yield of NO times the mass of an individual NO molecule.

$$M_{NO_P} = N_{NO_P} \, m_{NO} \tag{6.3}$$

6.2 Secondary Production of NO

After the impactor has contacted the ground, a large amount of earth is ejected. For simplicity we will assume the entire mass of the impactor is vaporized and ejected along with the ejected target forming a conical plume originating at the impact site [Zahnle, 1990]. Regions where the hypervelocity plume shocks the nitrogen and oxygen hard enough to form NO but weak enough to not subsequently eject this material permanently into space is discussed here.

First we must establish the post-shock target velocity (u_t) and post-shock impactor velocity (u_i). These velocities are dependent on the initial velocity of the impactor and the ratio of the target and impactor densities [Zahnle, 1990].

$$u_t = \frac{v_i}{1 + \left(\frac{\rho_t}{\rho_i}\right)^{\frac{1}{2}}} \tag{6.4}$$

$$u_i = \frac{v_i}{1 + \left(\frac{\rho_i}{\rho_t}\right)^{\frac{1}{2}}} \tag{6.5}$$

where ρ_t is the density of of target material and ρ_i is the density of of impactor

material.

Next it will be useful to define the mass of shocked target material, similarly this mass depends only on the mass of the impactor and the densities of the target and impactor.

$$M_t = M_i \left(\frac{\rho_t}{\rho_i} \right)^{\frac{1}{2}} \tag{6.6}$$

We also require the minimum post shock particle velocity for vaporization (u_v), this will determine how much of the shocked material is also vaporized. Provided by Zahnle [1990]:

$$u_v = \left(\frac{4\,Q_v}{h} \right)^{\frac{1}{2}} \tag{6.7}$$

where Q_v is the latent heat of vaporization of the impactor and h is a scale factor that is derived from crater scaling relations operating in the gravity regime. The quantity h can range from 0.4 Zel'dovich and Raizer [1967] to 0.8 Schmidt and Holsapple [1982]. This velocity is determined by the material itself and complete vaporization will occur everywhere the particle velocities (u_t and u_i) are greater than u_v.

Here it will be helpful to define a mass M_i' which will become in useful:

$$M_i' \equiv \frac{M_i\big(1 + (1-h)\frac{\rho_t}{\rho_i}\big)}{2-h} \tag{6.8}$$

After this point our calculations diverge depending on the whether the target is exposed land or covered in ocean.

6.2.1 Oceanic Impact

First we will define two more masses that will make our calculations easier:

$$\delta M_i = \pi \rho_w dr_i^2 \left(\frac{\rho_i}{\rho_w} \right) \tag{6.9}$$

where ρ_w is the mean density of sea water, and d is the depth of the ocean. δM_i can be thought of as the amount of impactor vaporized from impact with the ocean [Zahnle, 1990]. For large impacts this value is typically a small percentage of the total

impactor's mass.

$$\delta M_i' \equiv \frac{\delta M_i\left(1+(1-h)\frac{\rho_w}{\rho_i}\right)}{2-h} \tag{6.10}$$

Next we need to determine how much of the target is vaporized after travelling through the the water column.

$$M_{v_T} = \pi\,\rho_t\,d\,r_i^2\left(\frac{u_w}{u_i}\right)^{(2-h)} + \delta M_i'\left[\left(\frac{u_w}{u_i}\right)^{(2-h)} - 1\right] \tag{6.11}$$

The mass of vapor formed is the mass of vaporized target plus the mass of the remaining impactor after travelling through the ocean and impacting the ocean floor:

$$M_v = M_{v_T} + (M_i - \delta M_i) \tag{6.12}$$

Total energy left in the vapor plume is give by Zahnle [1990] as:

$$E_v = \frac{M_i - \delta M_i}{M_i}\left[\frac{h}{2}M_i\,u_i^2 + \frac{h}{2}\,M_t\,u_t^2 + \frac{2-h}{2}\,u_t^2\,(M_i+M_t)\left(1-\left(\frac{u_v}{u_t}\right)^h\right)\right] + E_{v_t} \tag{6.13}$$

The energy deposited into the vapor plume is equal to the kinetic energy given to the now vaporized target and terrestrial material plus the energy transformed into internal energy via shock plus E_{v_t}, the energy deposited into the target vapor as internal energy.

Where E_{v_t} is given by:

$$E_{v_t} = \frac{h}{2}\pi\rho_t\,d\,r_i^2\,u_t^2 + \frac{2-h}{2}\left(\delta M_i\,u_t^2 + \pi\,\rho_t\,d\,r_i^2\,u_t^2\right)\left[1-\left(\frac{u_v}{u_t}\right)^h\right] \tag{6.14}$$

6.2.2 Terrestrial Impact

For an impact striking land or a shallow sea, the mass of vapor formed (mostly target rock) is simply defined by Zahnle [1990] as:

$$M_v = M_i + M_t\left(\frac{u_t}{u_v}\right)^{(2-h)} + M_i'\left[\left(\frac{u_t}{u_v}\right)^{(2-h)} - 1\right] \tag{6.15}$$

Here you can see that we have assumed the impactor is capable of generating velocities large enough to form vapor, and during the impact the entire impactor was vaporized. The amount of vaporized target mass is proportional to the ratio of the post-shock target material and the minimum post shock particle velocity for vaporization to the power of two minus the scale factor. In addition their is a third term which relates the densities of the target and impactor with a complicated relationship with the scale factor.

With the above functions defined we can now solve for the amount of energy left in the vapor plume:

$$E_v = \frac{h}{2} M_i \, u_i^2 + \frac{h}{2} M_t \, u_t^2 + \frac{2-h}{2} \, u_t^2 \big(M_i' + M_t \big) \left[1 - \left(\frac{u_v}{u_t} \right)^h \right] \tag{6.16}$$

The first and second terms of the equation are the total thermal energies given to the vapor of what was once the impactor and the target respectively. The third term is the total internal energy transferred from the impactor material to the target material.

Now that we have the both the mass of vapor formed and the energy in the plume we can solve for the maximum velocity of the shock front. The formula provided by Zahnle [1990]:

$$v_{max} = \left(\frac{4\gamma}{(\gamma - 1)} \frac{E_v}{M_v} \right)^{\frac{1}{2}} \tag{6.17}$$

where once again γ is taken to be $9/7$.

In order to determine the total mass of NO produced during secondary production we require two more constants, A and α. Zahnle [1990] shows us that α can be determined relatively easily from the following formula:

$$\gamma = \frac{2\alpha + 5}{2\alpha - 1} \tag{6.18}$$

Once we have α, solving for A requires the use of conservation of energy, the initial thermal energy of the vapor and the final kinetic energy of the vapor are the same

[Zahnle, 1990]. The total vapor mass, E_v, can solved by the following:

$$E_v = 2\pi \int_0^{R_v} \frac{v^2}{2} \rho(r) r^2 dr \tag{6.19}$$

where R_v is the radius of the hemispherical plume and $\rho(r)$ is given by Zel'dovich & Raizer [1967]:

$$\rho(r) = \frac{A}{R_v^3} \left[1 - \left(\frac{r}{R_v} \right)^2 \right]^\alpha \tag{6.20}$$

Plugging in $\rho(r)$ and setting x $\equiv r/R_v = v/v_{max}$

$$E_v = \pi A \, v_{max}^2 \int_0^1 x^4 (1 - x^2)^\alpha dx \tag{6.21}$$

Once we have solved for A we can now solve for the cumulative mass in material with velocity greater than velocity v_{NO}, it should be noted that the following mass represents the amount of vaporized target and impactor material moving with velocity greater than velocity v_{NO}, not the amount of shocked atmosphere. Using Zahnle's formula:

$$M_{v>v_{NO}} = 2\pi A \int_{v_{NO}/v_{max}}^1 x^2 (1 - x^2)^\alpha dx \tag{6.22}$$

where v_{NO} is the minimum shock velocity required to produce NO and is given by Zel'dovich and Raizer [1967]:

$$v_{NO} = \left[\frac{2 \, m_{NO} \, T \, (\gamma - 1)}{k_b \, (\gamma + 1)} \right] \tag{6.23}$$

where once again T is the freeze out temperature, taken to be 1700 K, m_{NO} is the mass of a NO molecule, and k_b is the Boltzmann constant.

Now that we have the cumulative mass in material with velocity greater than velocity v_{NO} we must now determine how much momentum this plume imparts on the atmosphere.

$$p(v > v_{NO}) = 2\pi A \, v_{max} \int_{v_{NO}/v_{max}}^1 x^3 (1 - x^2)^\alpha dx \tag{6.24}$$

Zahnle then uses this result to calculate the total shocked atmospheric mass as:

$$M_{atm} = \frac{p(v > v_{NO})}{v_{NO}} - M_{v>v_{NO}} \tag{6.25}$$

Once we have the total mass atmosphere shocked with enough energy to produce NO, we can multiply that mass by the fraction of the atmosphere that is converted to NO via shock (Equation 1).

$$M_{NO_{S_T}} = f_{NO}(T)\, M_{atm} \tag{6.26}$$

Now we must remove the portion of NO that was ejected from the atmosphere and lost to space. To do this we return to equations 6.22, 6.24, 6.25, and 6.26 and replace every instance of v_{NO} with v_{esc}.

Eventually we end up with the total mass of NO that is shocked to a velocity greater than the escape velocity of Earth, this material is ejected from the atmosphere and does not return:

$$M_{NO_{S_{esc}}} = f_{NO}(T)\, M_{esc} \tag{6.27}$$

Subtracting the mass of NO in the atmosphere shocked with velocity greater than escape velocity from the total mass of NO produced gives us the total mass of NO produced that remains in the atmosphere.

$$M_{NO_S} = M_{NO_{S_T}} - M_{NO_{S_{esc}}} \tag{6.28}$$

6.3 Tertiary Production

As this ejected material begins to fall back to Earth it reenters the atmosphere globally, this results in global deposition of material. This material can be divided into three separate categories.

6.3.1 Ejecta Blanket

Although the ejecta blanket carries a considerable amount of mass it is neither ejected fast enough nor far enough to produce an appreciable fraction of NO [Zahnle,

1990]. Because of this the ejecta blanket will not be considered further.

6.3.2 Spalls

Spalls are lightly shocked rocks ejected at high velocity from the impact crater and if present will create NO on reentry. This material originates from the near surface target material, and thus spalls do not occur when an overlying deep ocean is present.

Zahnle argues that a reentering spacecraft should have a similar NO yield per erg as a reentering spall of similar size. He states that the observed NO yield per erg is approximately 10^{10} molecules of NO per erg. Thus if we know the total kinetic energy of all spall material we can determine the number of NO molecules formed during spall reentry.

The total kinetic energy of spalls is given by Zahnle [1990]:

$$KE_s = \frac{3M_i P_{max} v_i}{7\rho_t \beta C_L}\left[\left(\frac{v_1}{v_i}\right)^{7/3} - \left(\frac{v_2}{v_i}\right)^{7/3}\right] \tag{6.29}$$

where P_{max} is the Hugoniot Elastic Limit, spalls experiencing pressures greater than this are greatly shocked and pulverized [Zahnle, 1990], β is a parameter that describes the relationship between the ratio of decay time to the rise time of the shock wave [Zahnle, 1990], C_L is a constant with dimensions of velocity. v_1 is the upper limit of the velocity, it is either v_{esc} or $v_i/2$, which ever is smallest [Zahnle, 1990]. In our case v_{esc} is used for comets and $v_i/2$ is used for asteroids. v_2 is the minimum velocity required to produce NO, which is of course v_{NO}.

$$N_{NO_s} = P(NO_s)\, KE_s \tag{6.30}$$

Following our previous steps, the total mass of NO molecules produced is just the number of NO molecules multiplied by the mass of an individual NO molecule.

$$M_{NO_s} = N_{NO_s}\, m_{NO} \tag{6.31}$$

6.3.3 Condensates

As the rock vapor plume cools and condenses much of the material begins to rain back down onto Earth, although a small fraction of this material may reach escape

velocity, to first order this material all comes back to Earth [Zahnle, 1990]. Determining the mass of NO produced by these condensates requires a few assumptions. We will assume the average condensate radii is 0.01 cm. This result is provided to us by research conducted by Melosh [1982]. We will also assume the vapor plume velocity is approximately 10^5 cm/s and doesn't lose much energy travelling through the thin atmosphere as suggested by [Toon & Lawless , 1994]. Because of this simplification the plume and condensate parameters are identical.

The total mass of condensates is given by Toon & Lawless [1994]:

$$M_v = M_i \left[2 \left(\frac{4}{v_i} \left(\frac{Q_v}{\eta} \right)^{1/2} \right)^{\eta - 2} - 1 \right] \tag{6.32}$$

where η is a constant of about 0.33 [Toon & Lawless , 1994].

Now that we have the plume velocity and its corresponding mass we can determine the kinetic energy held within the condensates.

A further assumption needs to be made here; the entire mass of the falling condensates is effectively stopped once they encounter their own weight in atmosphere. Assuming silicate condensates as proposed by Zahnle, and knowing the droplets' average radii allows up to determine a condensates mass. The mass is much much less than the column of air the condensate would have encountered along its path down to the surface. This means that the condensates effective deposit all of their energy into the atmosphere.

$$KE_p = KE_v = KE_c = \frac{1}{2} M_v v_p^2 \tag{6.33}$$

According to Zahnle, because our condensates are stopped by the atmosphere, rather than the surface, our equation for the NO abundance, f_{NO}, changes to the following:

$$f_{NO}(T) = 6.8 \times 10^{-5} \, T \, e^{\frac{-3150}{T}} \tag{6.34}$$

From Zahnle we can now get the total number of molecules of NO produced by tertiary production:

$$N_{NO_c} = \frac{(\gamma - 1)}{k\,T} f_{NO}(T) K E_v \tag{6.35}$$

And of course the mass is just:

$$M_{NO_c} = N_{NO_c}\, m_{NO} \tag{6.36}$$

6.3.4 Tertiary Production of NO

The total mass of NO molecules produced via tertiary production is simply the sum of both the mass of NO molecules produced by spalls and the mass of NO produced by condensates:

$$M_{NO_T} = M_{NO_s} + M_{NO_c} \tag{6.37}$$

6.4 Total NO Production

The total production is simply the sum of the primary, secondary and tertiary production:

$$M_{NO} = M_{NO_P} + M_{NO_S} + M_{NO_T} \tag{6.38}$$

6.5 Creation of Tropospheric Ozone

Assuming NO atmospheric concentrations are greater than 5 ppt (parts per trillion), only 7.55×10^9 g, the following reactions result in a net positive ozone production in the troposphere [Crutzen, 2003].

Table 13: NO Reaction Sequence

Symbol	Reaction
R_1	$CO + OH \rightarrow H + CO_2$
R_2	$H + O_2 + M \rightarrow HO_2 + M$
R_3	$HO_2 + NO \rightarrow HO + NO_2$
R_4	$NO_2 + \gamma \rightarrow NO + O$
R_5	$O + O_2 + M \rightarrow O_3 + M$

Where M is inert, normally N_2 or O_2, but could also be a noble gas such as He or Ar [Mandelshtam et al., 1996].

Normally NO is the limiting molecule in this reaction series, however with NO flooding the region at levels approximately a billion times the atmospheric norm, CO becomes the limiting reactant [Mandelshtam et al., 1996]. It should be noted that although OH has a lower number density compared to CO and NO, its lifetime in the atmosphere is less than a second and it is constantly being replenished via OH recycling [Isaksen & Dalsøren 2011].

Crutzen [2003] notes that O_3 production is produced at a rate of 1:1 with the CO reservoir. Unfortunately Late Paleocene CO concentrations do not currently exist in the literature, instead we use the modern number density of CO outside of cities as a proxy for PETM CO number density. With this value we can estimate the creation of 80 ppb of O_3. It should be noted that this number density of CO may very well increase by the deposition of carbon from the impactor and this calculation represents a near lower limit for O_3 production. This massive over saturation of NO would disperse globally on the order years to tens of year [Zahnle, 1990]. Even for our lowest yield of NO generation, global concentrations would still be approximately equal to that of CO or over 10 times greater. Thus the total O_3 production would be on the order of the total CO in the atmosphere at the time of the PETM.

$$M_{O_3} = n_{CO} M_{atm} \tag{6.39}$$

where M_{O_3} is the total mass of O_3 created and M_{atm} is the mass of the entire modern atmosphere, where we are assuming the mass of the atmosphere has changed little since the PETM.

As stated previously O_3 has a GWP of 69 times that of CO_2 thus we can determine the equivalent mass of CO_2:

$$M_{EQ_{CO_2}} = \mathrm{GWP}_{O_3} M_{O_3} \tag{6.40}$$

where $M_{EQ_{CO_2}}$ represents the equivalent mass of CO_2 to create the equivalent GWP.

Table 14: List of Constants

Symbol	Variable	Value
T	Freeze Out Temperature	1700 K
N_A	Avogadro's Number	6.0221409×10^{23}
f_{N_2}	Paleocene Nitrogen Fraction	0.775
f_{O_2}	Paleocene Oxygen Fraction	0.225
d	Average Ocean Depth	3.688×10^{5} cm
n	Atmospheric Number density at Sea Level	2.504×10^{19} cm^{-3}
P	Atmospheric Pressure	1.01325×10^{6} Ba
ρ	Atmospheric Density	0.001225 g/cm^3
g	Acceleration due to Gravity	980.665 cm/s^2
H	Atmospheric Scale Height	8.5×10^{5} cm
Γ	Drag Coefficient	0.5
γ	NO Gas Constant at 1700 K	9/7
m_{no}	Mass of NO Molecule	5.02218×10^{-23} g
Q_i	Latent Heat of Vaporization of Ice	2.5×10^{10} ergs/g
Q_r	Latent Heat of Vaporization of Rock	8.0×10^{10} ergs/g
ρ_i	Density of Asteroid	2.865 g/cm^3
ρ_i	Density of Comet	0.6 g/cm
R	Radius of Earth	6.378×10^{8} cm
v_{esc}	Escape Velocity of Earth	1.118×10^{6} cm/s
ρ_t	Target Crustal Density	2.93 g/cm^3
P_{max}	Hugoniot Elastic Limit	4.5×10^{10} Ba
r_c	Radius of Condensates	0.01 cm
ρ_{sw}	Average Density of Sea Water	1.028 g/cm^3
C_L	Constant	6×10^{5} cm/s
β	Constant	4
M_{ATM}	Total Atmospheric Mass	$1.51\times10^{2}1$ g
n_0	Paleocene CO_2 concentration	500 ppm
n_{CO}	atmospheric number density of CO	8×10^{-8} cm^{-3}
GWP_{O_3}	GWP of O_3	69
GWP_{H_2O}	GWP of H_2O	5×10^{-4}
M_{bc}	Total Mass of Biogenic Carbon on Earth	9×10^{17} g
A_c	Total Continental Land Area	1.49×10^{18} cm^2
m_O	Mass of Oxygen Atom	2.6566962×10^{-23} g
m_C	Mass of Carbon Atom	1.9944235×10^{-23} g

Table 15: List of Variables

Symbol	Variable	Minimum Value	Maximum Value
σ_i	Ablation Parameter for Ice	6.4×10^{-12}	9.6×10^{-12}
σ_r	Ablation Parameter for Rock	2.0×10^{-12}	3.0×10^{-12}
v_i	Velocity of Asteroid	1.1×10^{6} cm/s	1.7×10^{6} cm/s
v_i	Velocity of Comet	5.1×10^{6} cm/s	7.2×10^{6} cm/s
M_i	Mass of Asteroid	1.875×10^{17} g	1.5×10^{18} g
M_i	Mass of Comet	$\frac{\pi}{8}\times10^{17}$ g	$\pi\times10^{18}$ g
r	Radius of Impactor	2.5×10^{5} cm	5×10^{5} cm
h	Scale Factor	0.4	0.8

7. Bibliography

Alvarez, Luis & Alvarez, Walter & Asaro, Frank & V. Michel, Helen. (1980). Extraterrestrial Cause for the Cretaceous-Tertiary Extinction. Science (New York, N.Y.). 208. 1095-108. 10.1126/science.208.4448.1095.

Archer, Dan & Eby, Michael & Brovkin, Victor & Ridgwell, Andy & Cao, Long & Mikolajewicz, Uwe & Caldeira, Ken & Matsumoto, Katsumi & Munhoven, Guy & Montenegro, Alvaro & Tokos, Kathy. (2009). Atmospheric Lifetime of Fossil Fuel Carbon Dioxide. Annual Review of Earth and Planetary Sciences, v.37, 117-134 (2009). 37. 10.1146/annurev.earth.031208.100206.

Artemieva, Natalia & Morgan, Joanna & Wittmann, Axel. (2017). Quantifying the Release of Climate-Active Gases by Large Meteorite Impacts With a Case Study of Chicxulub: Release of Climate-Active Gases. Geophysical Research Letters. 44. 10.1002/2017GL074879.

Aubry, M.-P., Ouda, Kh., Dupuis, C., Berggren, W. A., Van Couvering, J. A., and the Members of the Working Group on the Paleocene/Eocene Boundary. (2007). Global Standard Stratotype-section and Point (GSSP) for the base of the Eocene Series in the Dababiya Section (Egypt). Episodes, 30: 271-286.

Bar-On, Yinon & Phillips, Rob & Milo, Ron. (2018). The biomass distribution on Earth. Proceedings of the National Academy of Sciences. 115. 201711842. 10.1073/pnas.1711842115. https://www.liebertpub.com/doi/pdf/10.1089/ars.2017.7083.

Berner, Robert. (1990). Atmospheric Carbon Dioxide Levels Over Phanerozoic Time. Science (New York, N.Y.). 249. 1382-6. 10.1126/science.249.4975.1382.

Bowen, Gabriel & J. Maibauer, Bianca & Kraus, Mary & RÃűhl, Ursula & Westerhold, Thomas & Steimke, Amy & Gingerich, Philip & Wing, Scott & Clyde, William. (2014). Two massive, rapid releases of carbon during le onset of the Palaeocene-Eocene thermal maximum. Nature Geosciences. Online. 10.1038/ngeo2316.

Bralower, T & J. Thomas, D & Zachos, J.C. & Hirschmann, Marc & RÃűhl, Ursula & Sigurdsson, Haraldur & Thomas, Ellen & Whitney, Donna. (1997). High-resolution records of the late Paleocene thermal maximum and circum-Caribbean volcanism: Is there a causal link?.Geology.25.10.1130/0091-7613(1997)025<0963:HRROTL>2.3.CO;2.

Britt, Daniel & J. Consolmagno, G & Merline, William. (2006). Small Body Density and Porosity: New Data, New Insights.

Carozza, David & A. Mysak, Lawrence & Schmidt, Gavin. (2011). Methane and environmental change during the Paleocene-Eocene Thermal maximum (PETM): Modeling the PETM onset as a two-stage event. Geophysical Research Letters - GEOPHYS RES LETT. 38. 10.1029/2010GL046038.

Charles, Adam & Condon, Daniel & Harding, Ian & Paelike, Heiko & Marshall, John & Cui, Ying & Kump, Lee & Croudace, Ian. (2011). Constraints on the numerical age of the Paleocene-Eocene boundary. Geochemistry Geophysics Geosystems. 12. 10.1029/2010gc003426.

Collins, Gareth & Melosh, Jay & Marcus, Robert. (2005). Earth Impact Effects Program: A Web-based computer program for calculating the regional environmental consequences of a meteoroid impact on Earth. Meteoritics & Planetary Science. 40. 817 - 840. 10.1111/j.1945-5100.2005.tb00157.x.

Collinson, M.E. & Hooker, J.J. & Gröcke, Darren. (2003). Cobham Lignite Bed and penecontemporaneous macrofloras of southern England: A record of vegetation and fire across the Paleocene-Eocene Thermal Maximum. Causes and Consequences of Globally Warm Climates in the Early Paleogene. 369. 333-349. 10.1130/0-8137-2369-8.333.

Crovisier, J & Bockelée-Morvan, D. (1999). Remote Observations of the Composition of Cometary Volatiles. Space Science Reviews - SPACE SCI REV. 90. 19-32. 10.1023/A:1005217224240.

Crutzen, Paul. (2003). The Role of NO and NO_2 in the Chemistry of the Troposphere and Stratosphere. Annual Review of Earth and Planetary Sciences. 7. 443-472. 10.1146/annurev.ea.07.050179.002303.

Dickens G. R., M. M. Castillo, and J. C. G. Walker (1997), A blast of gas in the latest Paleocene: Simulating first-order effects of massive dissociation of oceanic methane clathrate, Geology, 25, 259-262.

Faure, G., & Mensing, T. M. (2005). Isotopes: Principles and Applications (3rd ed.). Hoboken, N.J: Wiley, c2005.

Hildebrand, Alan & T Penfield, Glen & A Kring, David & Pilkington, Mark & Camargo, Zuleica & Jacobsen, Stein. (1991). Chicxulub Crater: A possible Cretaceous/Tertiary boundary impact crater on the Yucatan Peninsula, Mexico. Geology. 19. 867-871. 10.1130/0 091-7613(1991)019<0867:CCAPCT>2.3.CO;2.

Hoffmann, Roald. (2006). Old gas, new gas. American Scientist.94.16.10.1511/2006.57.3476.

Holleman, A. F.; Wiberg, E. (2001) Inorganic Chemistry. Academic Press: San Diego.ISBN 0-12-352651-5.

Hunt, J. M. (1972). Distribution of Carbon in Crust of Earth. American Association of Petroleum Geologists, 56(11), 4.

Hunter, James & Bliss, Harding. (2002). Thermodynamic Properties of Aqueous Salt Solutions. Industrial & Engineering Chemistry. 36. 10.1021/ie50418a019.

Isaksen, I & Dalsøren, Stig. (2011). Getting a Better Estimate of an Atmospheric Radical. Science. 331. 38-39. 10.1126/science.1199773.

Jarosewich E. (1990) Chemical analyses of meteorites: a compilation of stony and iron meteorite analyses. Meteoritics 25, 323-337. doi:10.1111/j.1945-5100.1990.tb00717.x.

Kahn, A., & Aubry, M.-P. (2004). Provincialism in the calcareous nannoplankton during the PaleoceneEocene thermal maximum: constrain on timing and duration. Marine Micropalentology, 52: 117-131.

Kennett, J. P., Cannariato, K. G., Hendy, I. L., & Behl, R. J. (2003). Methane Hydrates in Quaternary Climate Change: The Clathrate Gun Hypothesis: American Geophysical Union.

Kennett, J. P., & Stott, L. D. (1991). Abrupt deep-sea warming, palaeoceanographic changes and benthic extinctions at the end of the Palaeocene. Nature, 353(6341), 225âĂŞ229. doi:10.1038/353225a0

Kent, Dennis & Cramer, Benjamin & Lanci, Luca & Wang, D & Wright, James & Van der Voo, Rob. (2003). A case for a comet impact trigger for the Paleocene/Eocene thermal maximum and carbon isotope excursion. Earth and Planetary Science Letters. 211. 13-26. 10.1016/S0012-821X(03)00188-2.

Kent, Dennis & Lanci, Luca & Wang, Huapei & Wright, James. (2017). Enhanced magnetization of the Marlboro Clay as a product of soil pyrogenesis at the Paleocene-Eocene boundary?. Earth and Planetary Science Letters. 473. 303-312. 10.1016/j.epsl.2017.06.014.

Kiehl, Jeffrey & E. Trenberth, Kevin. (1997). Earth's Annual Global Mean Energy Budget. Bulletin of the American Meteorological Society. 78. 10.1175/1520-0477(1997)078<0197:EAG MEB>2.0.CO;2.

Lawver, L.A., Dalziel, I.W.D., Norton, I.O., Gahagan, L.M., and Davis, J. "The PLATES 2014 Atlas of Plate Reconstructions (550 Ma to Present Day), PLATES Progress Report No. 374-0215." University of Texas Institute for Geophysics Technical Report No. 202 (February 2015), 220p.

Mandelshtam, Vladimir & Taylor, Howard & H. Miller, William. (1996). Collisional recombination reaction $H+O2+MHO2+M$: Quantum mechanical study using filter diagonalization. The Journal of Chemical Physics. 105. 496-503. 10.1063/1.471903.

Melosh, H. J. (1982). The mechanics of large meteoroid impacts in the Earth's oceans, in Silver, L. T., and Schultz, P. H., eds., Geological implications of impacts of large asteroids and comets on the Earth: Geological Society of America Special Paper 190, p. 121-127.

McInerney, Francesca & Wing, Scott. (2011). The Paleocene-Eocene Thermal Maximum: A Perturbation of Carbon Cycle, Climate, and Biosphere with Implications

for the Future. Annu. Rev. Earth Planet. Sci.. 39. 489-516. 10.1146/annurev-earth-040610-133431.

Mollenhauer, Gesine & Kienast, Markus & Lamy, Frank & Meggers, Helge & R. Schneider, Ralph & Hayes, John & Eglinton, Timothy. (2005). An evaluation of 14C age relationships between co-occurring foraminifera, alkenones, and total organic carbon in continental margin sediments. Paleoceanography. 20. 10.1029/2004PA001103.

Monroe, J. S., & Wicander, R. (2001). The changing earth: Exploring geology and evolution. Pacific Grove, CA: Brooks/Cole.

Myhre, Gunnar & Highwood, Eleanor & P. Shine, Keith & Stordal, Frode. (1998). New estimtes of raditive forcing due to well mixed greenhouse gases. Geophysical Research Letters. 25. 2715-2718. 10.1029/98GL01908.

Pagani, Mark & Pedentchouk, N & Huber, Matthew & Sluijs, Appy & Schouten, Stefan & Brinkhuis, Henk & Sinninghe-Damste, J & Reichart, G.-J & Dickens, Gerald. (2006). Arctic hydrology during global warming at the Paleocene/Eocene Thermal Maximum. Nature. 442. 10.1038/nature05043.

Patterson, Michael & Francis, Don. (2013). Kimberlite eruptions as triggers for early Cenozoic hyperthermals. Geochemistry, Geophysics, Geosystems.14.448-456.10.1002/ggge.20054.

Pearson, Victoria & Sephton, Mark & Franchi, Ian & Gibson, Jennifer & Gilmour, Iain. (2006). Carbon and nitrogen in carbonaceous chondrites: Elemental abundances and stable isotopic compositions. Meteoritics and Planetary Science. 41. 10.1111/j.1945-5100.2006.tb00 459.x.

Renne, Paul & L Deino, Alan & Hilgen, Frits & Kuiper, K.F. & F Mark, Darren & S Mitchell, William & Morgan, Leah & Mundil, Roland & Smit, Jan. (2013). Time Scales of Critical Events Around the Cretaceous-Paleogene Boundary. Science (New York, N.Y.). 339. 684-7. 10.1126/science.1230492.

Retallack, Gregory. (1997). Neogene Expansion of the North American Prairie. PALAIOS. 12. 380. 10.2307/3515337.

Schmidt, R. M., & Holsapple, K. A. (1982). Estimates of crater size for large body impact, in Silver, L. T., and Schultz, P. H., eds., Geological implications of impacts of large asteroids and comets on the Earth: Geological Society of America Special Paper 190, p. 93-102.

Schmitz, Birger & Pujalte, Victoriano. (2003). Sea-level, humidity, and land-erosion records across the initial Eocene thermal maximum from a continental-marine transect in northern Spain. Geology. 31. 10.1130/G19527.1.

Sherwood, Steven & Dixit, Vishal & Salomez, Chryséis. (2018). The global warming potential of near-surface emitted water vapour. Environmental Research Letters. 13. 10.1088/1748-9326/aae018.

Silver, L. T., & Schultz, P. H. (1982). Geological Implications of Impacts of Large Asteroids and Comets on the Earth. Geological Society of America, 190. doi:https://doi.org/10.1130/SPE190.

Sluijs, Appy & Schouten, Stefan & Pagani, Mark & Woltering, Martijn & Brinkhuis, Henk & Sinninghe-Damste, J & Dickens, Gerald & Huber, Matthew & Reichart, Gert-Jan & Stein, Ruediger & Matthiessen, Jens & Lourens, Lucas & Pedentchouk, N & Backman, Jan & Moran, Kathryn. (2006). Subtropical Arctic Ocean temperatures during the Paleocene/Eocene thermal maximum. Nature. 441. 610-3. 10.1038/nature04668.

Smith, Thierry & Rose, Kenneth & Gingerich, Philip. (2006). Rapid Asia-Europe North America geographic dispersal of earliest Eocene primate Teilhardina during the Paleocene-Eocene Thermal Maximum. Proc. Natl. Acad. Sci. USA 103, 11223-11227. Proceedings of the National Academy of Sciences of the United States of America. 103. 11223-7. 10.1073/pnas.0511296103.

Storey, Michael & Duncan, Robert & C Swisher, Carl. (2007). Paleocene-Eocene Thermal Maximum and the Opening of the Northeast Atlantic. Science (New York, N.Y.). 316. 587-9. 10.1126/science.1135274.

Svensen, Henrik & Planke, Sverre & Malthe-SÃ¿renssen, Anders & Jamtveit, Bjorn & Myklebust, Reidun & Rasmussen Eidem, Torfinn & Rey, Sebastian. (2004). Release of methane from a volcanic basin as a mechanism for initial Eocene global warming. Nature. 429. 542-5. 10.1038/nature02566.

Central Intelligence Agency. (2018). The World Factbook: World.

Thomas, E. (1998). The biogeography of the late Paleocene benthic foraminiferal extinction, In: M.-P. Aubry, S. Lucas, and W. A. Berggren, eds., Late Paleocene-early Eocene Biotic and Climatic Events in the Marine and Terrestrial Records, Columbia University Press, 214-243.

Toon, Owen & G. Lawless, James. (1994). Environmental Perturbations Caused by the Impacts of Comets and Asteroids on Earth. Rev.Geophys..35.10.1029/96RG03038.

Weast, Robert C. CRC Handbook of Chemistry and Physics 48th edtion. Chemical Rubber Co., 1968: F-135.

Woods, Thomas & D. Feldman, P & Dymond, Kenneth & J. Sahnow, D. (1987). Rocket ultraviolet spectroscopy of comet Halley and abundance of carbon monoxide and carbon. Nature. 324. 10.1038/324436a0.

Wright, James& Schaller, Morgan. (2013). Evidence for a rapid release of carbon at the Paleocene-Eocene Thermal Maximum. Proceedings of the National Academy of Sciences of the United States of America. 110. 10.1073/pnas.1309188110.

Zachos, J.C. & Röhl, Ursula & Schellenberg, S.A. & Sluijs, Appy & A Hodell, David & C Kelly, Daniel & Thomas, Ellen & Nicolo, Micah & Raffi, Isabella & Lourens, Lucas & McCarren, Heather & Kroon, Dick. (2005). Paleoclimate: Rapid acidification of the ocean during the paleocene-eocene thermal maximum. Science. 308. 10.1126/science.1109004.

Zachos, J.C. & Dickens, Gerald & E Zeebe, Richard. (2008). An Early Cenozoic perspective on Greenhouse warming and carbon cycle dynamics. Nature. 451. 279-83. 10.1038/nature06588.

Zahnle KJ. (1990). Atmospheric chemistry by large impacts. In Global Catastrophes in Earth History. Sharpton V., Ward P., Eds., GSA Special Paper; 247: 271-288.

Zel'dovich, Ya. B., and Raizer, Yu. P. (1967) Physics of shock waves and high temperature hydrodynamic phenomena: New York, Academic Press, 916 p.